

The cascade unzipping of ladderane reveals dynamic effects in mechanochemistry

Zhixing Chen^{1,4}, Xiaolei Zhu^{1,2,4}, Jinghui Yang¹, Jaron A. M. Mercer¹, Noah Z. Burns¹, Todd J. Martinez^{1,2,3*} and Yan Xia^{1*}

Force can induce remarkable non-destructive transformations along a polymer, but we have a limited understanding of the energy transduction and product distribution in tandem mechanochemical reactions. Ladderanes consist of multiple fused cyclobutane rings and have recently been used as monomeric motifs to develop polymers that drastically change their properties in response to force. Here we show that [4]-ladderane always exhibits 'all-or-none' cascade mechanoactivations and the same stereochemical distribution of the generated dienes under various conditions and within different polymer backbones. Transition state theory fails to capture the reaction kinetics and explain the observed stereochemical distributions. Ab initio steered molecular dynamics reveals unique non-equilibrium dynamic effects: energy transduction from the first cycloreversion substantially accelerates the second cycloreversion, and bifurcation on the force-modified potential energy surface leads to the product distributions. Our findings illustrate the rich chemistry in closely coupled multi-mechanophores and an exciting potential for effective energy transduction in tandem mechanochemical reactions.

Using polymers to apply mechanical force has been recognized in the last decade as an external means to direct non-destructive transformations on judiciously designed molecules, dubbed mechanophores, and has opened exciting avenues for developing novel materials that can sense, respond and adapt to external stress¹. Mechanical force can induce reaction pathways different from thermal or photochemical processes², stabilize reactive intermediates³, activate latent catalysts⁴, fluorescence^{5,6} and chemoluminescence^{7,8}, as well as release small molecules^{9,10} and generate acid¹¹ or stable radicals^{12,13}. Besides enabling unprecedented materials, polymer mechanochemistry has been investigated to reveal several unique mechanistic features that arise due to the force-modified potential energy surface, such as the lever-arm effect¹⁴, the generation of force-induced minima^{3,15,16} and the force-accelerated dissociation of unloaded bonds^{17,18}. Detailed understanding of mechanochemical pathways provides the foundation for future development of this new chemistry modality.

In the quest for polymers that dramatically transform their intrinsic properties in response to mechanical stimulation, we have developed a class of polyladderenes that undergo rapid force-triggered unzipping to transform into polyacetylene with a long conjugation length¹⁶. The repeating unit of polyladderene can be considered a unique multi-mechanophore consisting of a linear sequence of fused cyclobutane/ene rings, which have been shown to be privileged mechanophores in polymer mechanochemistry^{2,7,19–25}. The unzipping of [4]-ladderene involves two consecutive mechanochemical cycloreversion events of four-membered rings, with four bonds being broken. Interesting questions then arise regarding the tandem mechanochemical activations of closely coupled multi-mechanophores, as in ladderene/ane (Fig. 1). Understanding the mechanochemical behaviour of multi-mechanophores can provide insights into the mechanotransduction along covalent bonds and the design of multi-mechanophore systems with sensitive amplified response²⁶. The rapid unzipping and formation of insoluble

conjugated polyacetylene prohibits detailed interrogation of the sequence and stereochemistry of the mechanoactivation of individual ladderene units. Therefore, we embedded one or multiple units of ladderane in polymers with saturated backbones to break the extended conjugation and carefully analysed the sonochemical products using NMR spectroscopy and computation. We observed highly selective 'all-or-none' activation and an interesting stereochemical distribution of the formed olefins. This study provides important mechanistic insights into consecutive mechanoactivations to aid the future design of multi-mechanophores with potentially amplified response and controlled products.

Results and discussion

Tandem mechanochemistry of individual [4]-ladderene/ane. To understand the mechanochemical behaviour of an individual ladderene architecture, we first sought to synthesize ladderene/ane initiators using chloroladderene **1** in order to grow two long strands of polymers to incorporate the mechanophore in the middle of a polymer chain (Fig. 2a). Due to its rapid ring-opening metathesis polymerization (ROMP), we failed to derivatize **1** via ring-opening cross metathesis. Instead, ozonolysis of **1** with reductive work-up led to the [4]-chloroladderene diol **2** in moderate yield. Elimination of HCl afforded [4]-ladderene diol **3** in quantitative yield, which was then functionalized with initiators for atom transfer radical polymerization. We thus obtained high-molecular-weight poly(methyl acrylate) (PMA) with one ladderene unit embedded in the centre. Pleasingly, the terminal cyclobutene motif on the ladderene was preserved under the mild polymerization condition, as indicated by ¹H NMR spectroscopy (Fig. 2f).

We then investigated the mechanoactivation of chain-centred ladderene under ultrasonication in acetonitrile (Fig. 2b). Aliquots of the reaction mixture at selected time points were analysed by UV-vis spectroscopy. The starting polymer did not exhibit absorption above 250 nm, but three distinct absorption peaks at 316, 331

¹Department of Chemistry and Stanford University, Stanford, CA, USA. ²The PULSE Institute, Stanford University, Stanford, CA, USA. ³SLAC National Accelerator Laboratory, Menlo Park, CA, USA. ⁴These authors contributed equally: Zhixing Chen, Xiaolei Zhu. *e-mail: toddmtz@stanford.edu; yanx@stanford.edu

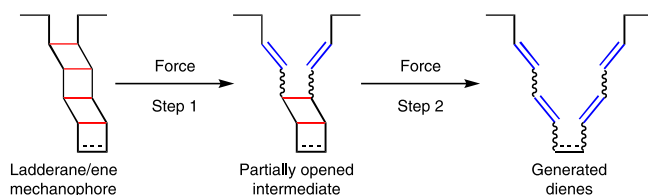


Fig. 1 | The mechanochemistry of ladderane/ene consists of tandem cycloreversions. Key mechanistic questions include (1) whether there is cooperativity in the tandem mechanochemical steps and (2) what determines the stereochemistry of olefin products.

and 348 nm emerged within 20 min of sonication (Fig. 2c). The wavelengths and vibronic pattern of the peaks are characteristic of a conjugated pentaene²⁷, as expected from complete unzipping of [4]-ladderene. The intensity of these peaks slightly increased after prolonged sonication to 60 min, but significantly decreased after 3 h of sonication, with concomitant growth of a broad peak between 260 and 300 nm. Ultrasonication is known to generate radicals²⁸, which we attributed to degradation of the formed pentaene, considering that oligoenes such as carotenoids are common radical scavengers²⁹.

To address the stability issue, we added 30 mM TEMPO as radical scavenger to the sonication solution and precipitated the polymer to remove the TEMPO before analysis. With the addition of TEMPO, we observed a steady increase in the intensity of the pentaene peaks on increasing the sonication time to 3 h (Fig. 2d). Raman microspectroscopy of the sonicated sample under 532 nm excitation exhibited a new signal at 1,585 cm⁻¹ (Fig. 2e), which corresponds to the predicted C=C stretching frequency in pentaene³⁰. The ¹H NMR spectrum of the activated PMA showed a significantly decreased vinyl proton signal at 6.3 ppm from ladderene **5** and the simultaneous appearance of signals in vinyl (5.6–5.8 and 6.2–6.4 ppm) and allylic (4.5–4.6 ppm) regions, corresponding to the reported pentaene NMR resonances (Fig. 2f)³¹. However, the relatively broad NMR signals of the resulting pentaene hampered detailed analysis of the stereochemistry of the formed olefins.

To interrogate the stereochemistry and confirm the absence of partially opened intermediate, we sought to break the continuous conjugation using [4]-ladderane as our target of investigation. A [4]-ladderane centred in high-molecular-weight PMA was synthesized using a procedure similar to that described above (Fig. 3a). Over the course of sonication, several ¹H NMR resonances emerged and intensified in the vinyl (5.4–5.8 ppm), diene (5.9–6.6 ppm) and allyl ester (4.5–4.6 ppm) regions, with a concomitant decrease in signal intensity for both the cyclobutane (2.6–2.9 ppm) and α -methylene of ladderane (4.1–4.3 ppm) (Fig. 3b,c). Comparing the integrations of the NMR signals, we observed that about half of the [4]-ladderane was activated in 3 h of sonication, along with a decrease in polymer molecular weight from 96 to 55 kDa, measured by gel permeation chromatography analysis (Supplementary Table 2).

To identify the stereochemistry of the formed olefins, we compared the emerged ¹H NMR signals from unzipped ladderane to those of model dienes and vinyl cyclobutane compounds (Supplementary Table 3). Accordingly, we assigned the formed olefinic resonances to a mixture of two dienes with *E,E* (major, ~80%) and *E,Z* (minor, ~20%) configurations, by matching the chemical shifts and coupling patterns with two synthesized model diene compounds, **I** and **II** (Fig. 3c). Notably, the relative intensities of the major and minor mechanochemical diene products remained constant throughout the course of 3 h sonication, suggesting that this product distribution resulted directly from ladderane mechanochemistry instead of subsequent *cis-trans* isomerization. Moreover, the ratio of *E,E* to *E,Z* diene products remained approximately 4:1 when sonication

was performed at a much lower temperature (–40 °C), in different solvents (CH₃CN and THF) and using PMA with several different molecular weights (56–110 kDa) (Supplementary Fig. 3). We also designed a multi-mechanophore polymer **15** containing many units of [4]-ladderane to significantly enhance the NMR signals from the single chain-centred mechanophore and most unambiguously confirm the mechanochemical product distribution. This polymer was synthesized by ROMP of a [4]-ladderane-containing macrocyclic olefin **14** and a substituted cyclooctene (Fig. 4). The cyclooctene comonomer was used to yield a high-molecular-weight (80 kDa) multi-mechanophore polymer and help to solubilize the activated polymer. Sonication of polymer **15** for 3 h resulted in 33% of the [4]-ladderane units being activated, giving rise to much more intense and well-resolved NMR signals with similar patterns to those from chain-centred mechanophore **11** (Fig. 4). The clear NMR signals allowed us to re-confirm the chemical shifts and coupling constants that corresponded to the *E,E* and *E,Z* dienes (Supplementary Figs. 4 and 5). Their relative integrations (most clearly from the comparison of the new allylic proton signals at 4.55–4.65 ppm) allowed us to precisely determine the product distribution to be 79 ± 1% *E,E* and 21 ± 1% *E,Z* products. The unambiguous assignments and perfect integrations of all the generated ¹H NMR peaks in olefinic and allylic regions also suggested the absence of the hypothetical singly ring-opened intermediate **13**, a 1,2-divinylcyclobutane structure. These interesting observations collectively revealed unique features in the mechanochemical unzipping of ladderane: (1) the unzipping of ladderane occurred in an ‘all-or-none’ manner, either remaining intact or unzipping completely; (2) the first cyclobutane cycloreversion formed all *E* olefins, where the initial stereochemistry was completely retained, while the second cyclobutane cycloreversion gave ~80% *E,E* and ~20% *E,Z* products.

Mechanistic insights into cascade unzipping of ladderane. The mechanochemistry of ladderane/ene features sequential activation events. Experimental observations of the cascade activation suggest a facilitated second cyclobutane cycloreversion. It is widely accepted that the mechanochemical cycloreversion of cyclobutane proceeds through a sequential bond rupture mechanism via a 1,4-diradical species^{16,19,23}. Our previous calculation on ladderene unzipping further confirmed that the transition states (TSs) on the force-modified potential energy surface (FMPES) are diradical structures¹⁶. The cascade unzipping behaviour of ladderane can be partly attributed to the lower thermodynamic barrier on the FMPES for the second cycloreversion due to stabilization of the radical TS by the generated olefins¹⁶.

However, on closely examining the two consecutive mechanochemical events, we discovered a striking dynamic effect—evidence for effective mechanotransduction in tandem mechanoactivations that also contributed to the cascade ladderane unzipping. We used ab initio steered molecular dynamics (AISMD) to investigate the reaction process, particularly the effect of the first cycloreversion on the second cycloreversion. Using AISMD, we computationally investigated the rate of mechanochemical cycloreversion of intermediate structure **19** when being pulled under thermal equilibrium as compared to the same structure being pulled as the second consecutive cycloreversion event during unzipping of ladderane **16**. This comparison would reveal any potential non-equilibrium dynamic effect in a tandem process, where the strain release and kinetic energy resulting from the first cycloreversion (**16** to **19**) could affect the rate of the second cycloreversion (**19** to **21/22**).

We compared the opening of structure **19** using AISMD under different forces from 1 to 3.1 nN for 50 ps at 300 K using UB3LYP/6–31g*. Geometry optimization and frequency analysis were performed to generate a 300 K harmonic Wigner distribution to serve as the initial conditions for AISMD simulations. An *n*-butyl group was added to each terminus of [4]-ladderane **16** in our

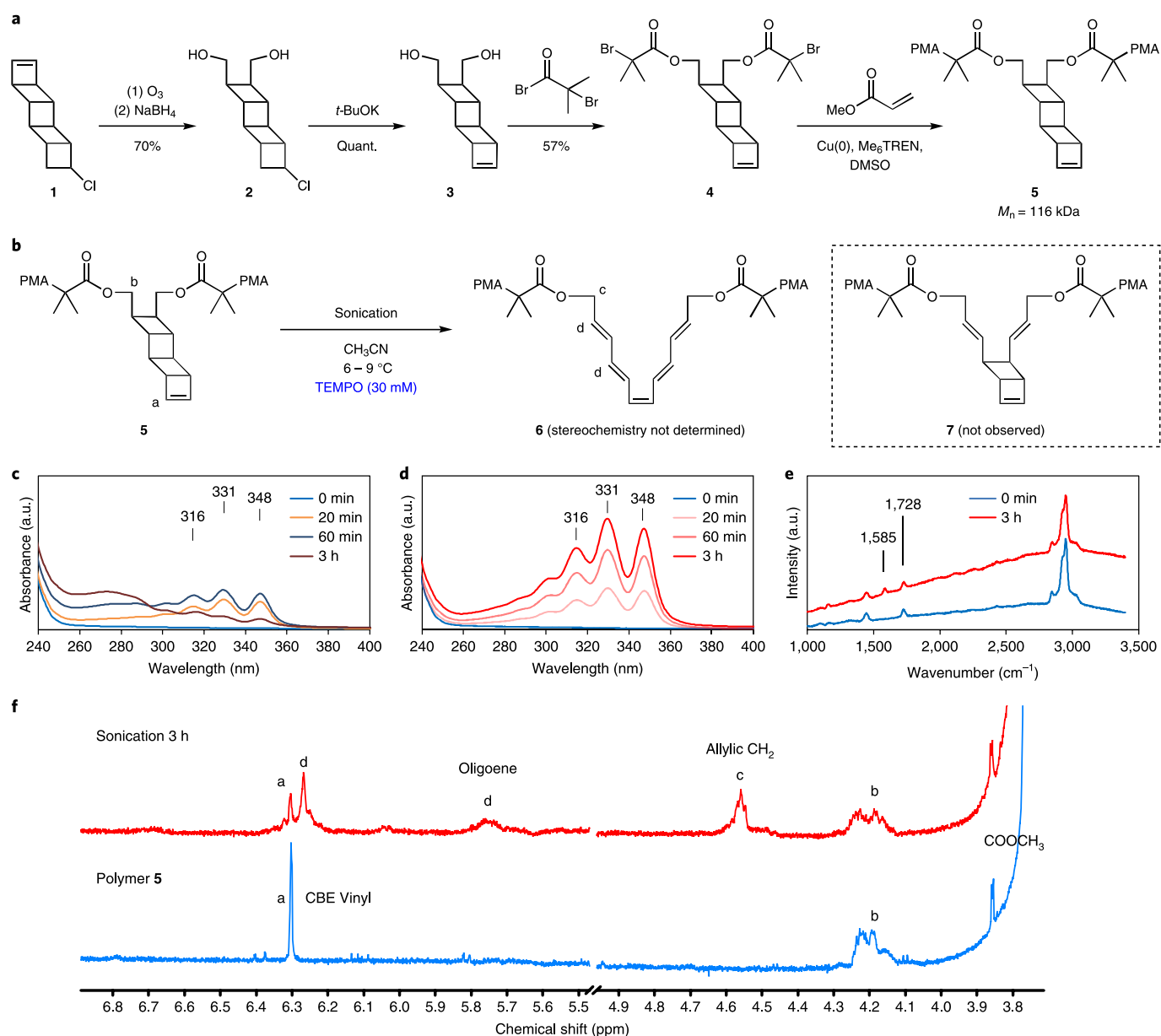


Fig. 2 | Mechanochemistry of chain-centred [4]-ladderene. **a**, Synthetic scheme for the [4]-ladderene initiator, which was used to grow two strands of polymers for the study of chain-centred mechanophore. **b**, Sonochemical activation of [4]-ladderene, leading to the fully unzipped product, pentaene. **c**, Ultraviolet absorption spectra of **5** before and after sonication, indicating degradation of the formed pentaene during sonication. **d**, Ultraviolet absorption spectra of **5** during sonication in the presence of 30 mM (2,2,6,6-tetramethylpiperidin-1-yl)oxyl (TEMPO) as radical scavenger, indicating stabilization of the formed pentaene. **e**, Raman microspectroscopy of **5** before and after sonication. **f**, $^1\text{H NMR}$ spectra of **5** before and after sonication (the methyl ester peak of PMA is normalized for scaling). All the spectroscopic evidence supports the formation of pentaene as the fully unzipped product.

calculations to minimize any possible linker effect when using short linkers (Supplementary Fig. 6)³². No mechanochemical reaction occurred for **16** under forces of $<2.9 \text{ nN}$ within the 50 ps timeframe of dynamic simulation. Therefore, we instead carried out dynamics sampled from a Wigner distribution centred on the TS structure **17[‡]** (see Supplementary Section 3.2 for details). AISMD showed that approximately half of the **17[‡]** population proceeded to give **21/22** through **19**, while the rest reverted to **16** (Supplementary Table 6), supporting the correct assignment of the TS. We probed the cycloreversion rate of **19** using dynamics that started from either thermally equilibrated **19** (red trajectory, Fig. 5b) or **17[‡]** (blue trajectory, Fig. 5b). The calculated fraction of remaining **19** as a

function of both force and reaction time showed that the cycloreversion of **19** was dramatically accelerated (occurring within 1 ps at forces exceeding 2 nN) when starting from **17[‡]** as compared to starting from equilibrated **19** (Fig. 5c,d). The monoexponential decay predicted by transition state theory (TST) was observed when the AISMD simulations started with equilibrated **19**, with a rate constant of 1.75 ns^{-1} at 2.5 nN of applied force (Supplementary Figs. 7 and 9; the procedure to compute rate constants from dynamics simulations is detailed in Supplementary Section 3.3). In contrast, a biexponential decay was observed when starting from **17[‡]**, with an additional ultrafast component due to reaction to **20** bypassing **19** (Supplementary Fig. 8). This is a dynamic effect and cannot be

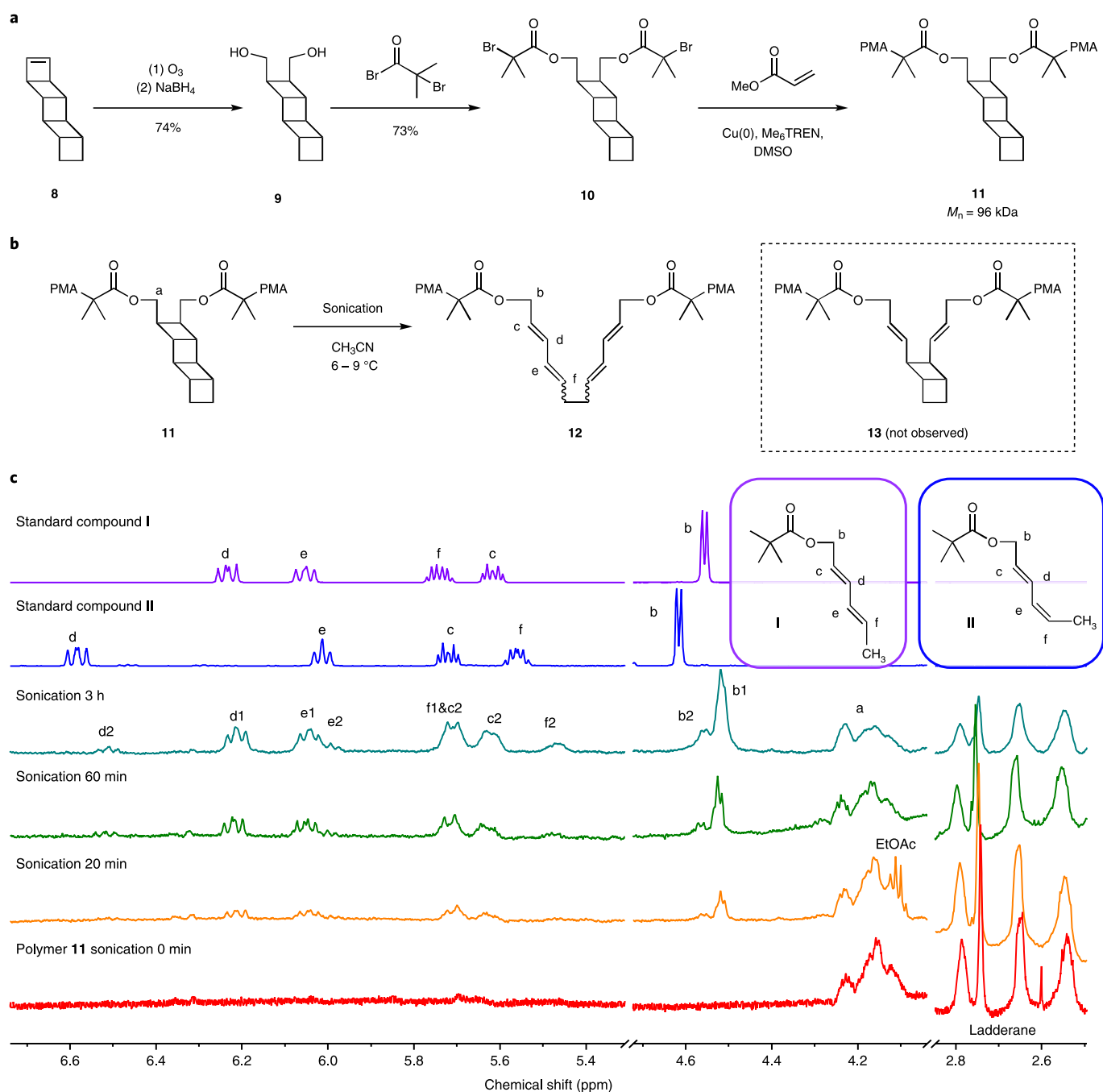


Fig. 3 | Mechanochemistry of chain-centred [4]-ladderene. **a**, Synthetic scheme for the [4]-ladderene initiator, which was used to grow two strands of polymers for the study of the chain-centred mechanophore. **b**, Sonochemical activation of [4]-ladderene, leading to a pair of dienes without half-opened species **13**. **c**, ^1H NMR spectra of polymer **11** over the course of sonication (the methyl ester peak of PMA is normalized for scaling) and comparison with the model diene compounds, indicating the absence of half-opened species and a stereochemical distribution of the formed pair of dienes in 80% *EE*, *EE* and 20% *EE*, *EZ* configurations.

modelled with conventional TST. The large kinetic energy released from the first mechanochemical event is partly transduced to significantly accelerate the second cycloreversion. A kinetic model of this process is described in Fig. 5f. Rate constants of the competing deactivation (k_{deact}) and direct reaction (k_{noneq}) processes of activated **19** (**19***) were extracted from the simulation (Supplementary Section 3.4 and Supplementary Fig. 10). The dynamic effect resulted in at least one order of magnitude acceleration of the second cycloreversion under 2–3 nN force (Supplementary Fig. 9). The effect of acceleration was more dramatic with increasing force. For example,

at 2.5 nN force, more than four orders of magnitude acceleration was achieved. The dynamic effect is most significant at relatively higher but still experimentally relevant forces when the mechanochemical reaction occurs within ~ 1 ps, due to limited dissipation of kinetic energy on this short timescale. This can be seen from the rapidly increasing fraction of **19** that undergoes the accelerated process as the force is increased beyond 2 nN (Fig. 5e). The rigid ladderane framework provides strong coupling between sequential mechanoactivations (minimal energy dissipation and well-aligned reaction coordinates) to allow energy transduction from the first

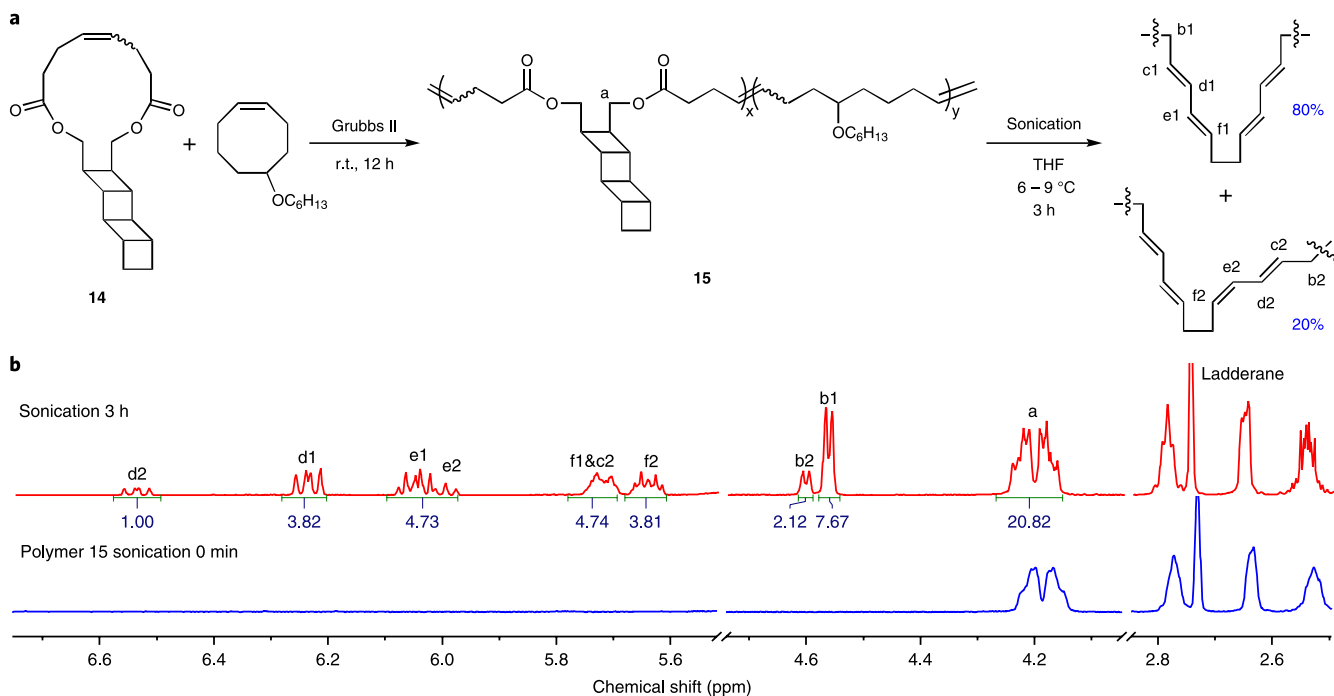


Fig. 4 | Mechanochemistry of a multi-mechanophore polymer containing multiple [4]-ladderane units. **a**, Synthesis and sonoactivation of a multi-mechanophore polymer, **15**. **b**, ^1H NMR spectra of polymer **15** before and after sonoactivation, unambiguously showing the all-or-none unzipping and the stereochemistry of the formed pair of dienes to be 80% *EE*, *EE* and 20% *EE*, *EZ*.

mechanochemical event to the subsequent mechanochemical event. This discovery represents an unambiguous example of a non-statistical dynamic effect in mechanochemistry, analogous to the ‘chemical activation’ in some thermally driven chemical reactions^{33–36}.

We next analysed the stereochemical distribution of the formed olefin products based on our AISMD calculations. For the first pair of formed olefins in **19**, pathways to both *Z* and *E* configurations were barrierless at >2 nN force, and there was no stable minimum for **18** (Supplementary Fig. 11). AISMD yielded only the *E* configuration (Supplementary Section 3.6), agreeing with the experimental observations. Such agreement suggests that the *E* selectivity is controlled by a dynamic effect, but the presence of only one product makes it difficult to investigate the branching behaviour on potential surface and reaction selectivity. We therefore focused our attention on the formation of the second pair of olefins. To understand the stereochemical distribution of the second pair of olefins, trajectory snapshots were binned based on the C–C distance and torsion angle shown in Fig. 6b (see Supplementary Section 3.7 for details of this procedure). Under each applied force, the minimum energy within each bin gives the effective FMPES, which is significantly different from the potential surface without applied force (Fig. 6c). Under 2 nN force, structure **20** formed a ‘caldera’^{37,38} on the FMPES with exit barriers of 2.99 and 2.13 kcal mol⁻¹ to **21** and **22**, respectively (Fig. 6d; see Supplementary Table 4 for barriers at other force levels). Thermodynamic analysis using harmonic frequencies and rotor approximations to low-frequency vibrations³⁹ yielded free energy corrections of -1.15 and -1.03 kcal mol⁻¹ for **21** and **22**, respectively (Supplementary Section 3.5, Supplementary Fig. 11 and Supplementary Table 5). Based on these energy barriers, TST predicts that the *Z* olefin would be the major product with $\sim 80\%$ yield, contradicting the observed product distribution. TST does not capture non-equilibrium dynamic effects, which can be significant for low-barrier reactions^{34,40}. At forces higher than 2.5 nN, the topology of the FMPES was fundamentally changed (Fig. 6e): the caldera corresponding to **20** and the TS leading to **21** and **22** vanished and were

replaced by a valley–ridge inflection (VRI) point^{41,42}, which leads to bifurcation of reaction pathways (Fig. 6f and Supplementary Fig. 13). Force-induced modification of potential energy surfaces leading to reaction pathway bifurcation has previously been demonstrated in cyclopropane mechanophores⁴³, and our further demonstration in the context of ladderanes suggests that the phenomenon may be general. The bifurcation is clearly visualized by the trajectories from AISMD simulations shown in Fig. 6f. As barriers significantly diminish, TST is not applicable and strong dynamic effects are expected. Capturing the dynamic effect, AISMD gave the *Z* olefin as a minor product around $24 \pm 14\%$ in a wide force range of 2–3 nN (Supplementary Fig. 12), closely agreeing with the experimental observations. We note that the 2–3 nN force range in our simulation is relevant to experimental values under sonochemical conditions⁴⁴. Additionally, the stereochemical distribution of the second pair of formed olefins appeared statistically similar, whether the cycloreversion started from **16** or **19** (Fig. 6a), at all simulated force levels of 2–3 nN. Therefore, the *E,Z* branching ratio is not dependent on acceleration from the preceding cycloreversion event, as discussed previously.

Analysis of AISMD trajectories revealed how the dynamic effect affects the product branching ratio. For each trajectory passing the VRI region under 3 nN force, we computed the torsion angles and the torsional velocities determining the *EZ* branching when the length of the breaking C–C bond exceeds 1.9 Å from **20** to **21/22** (Fig. 6g). This bond distance corresponds to the TS to form the two products. Using logistic regression, the phase space near the VRI was divided into two areas that correlate to the products. This simple linear classifier was found to be a good predictor, and the tilted boundary line showed that both the momentum and the torsion angle near the VRI determine the product distribution in the bifurcation process (see Supplementary Section 3.8 and Supplementary Figs. 14–16 for details). The area correlating to product **21** is much larger than that correlating to product **22**, agreeing with high selectivity towards **21**.

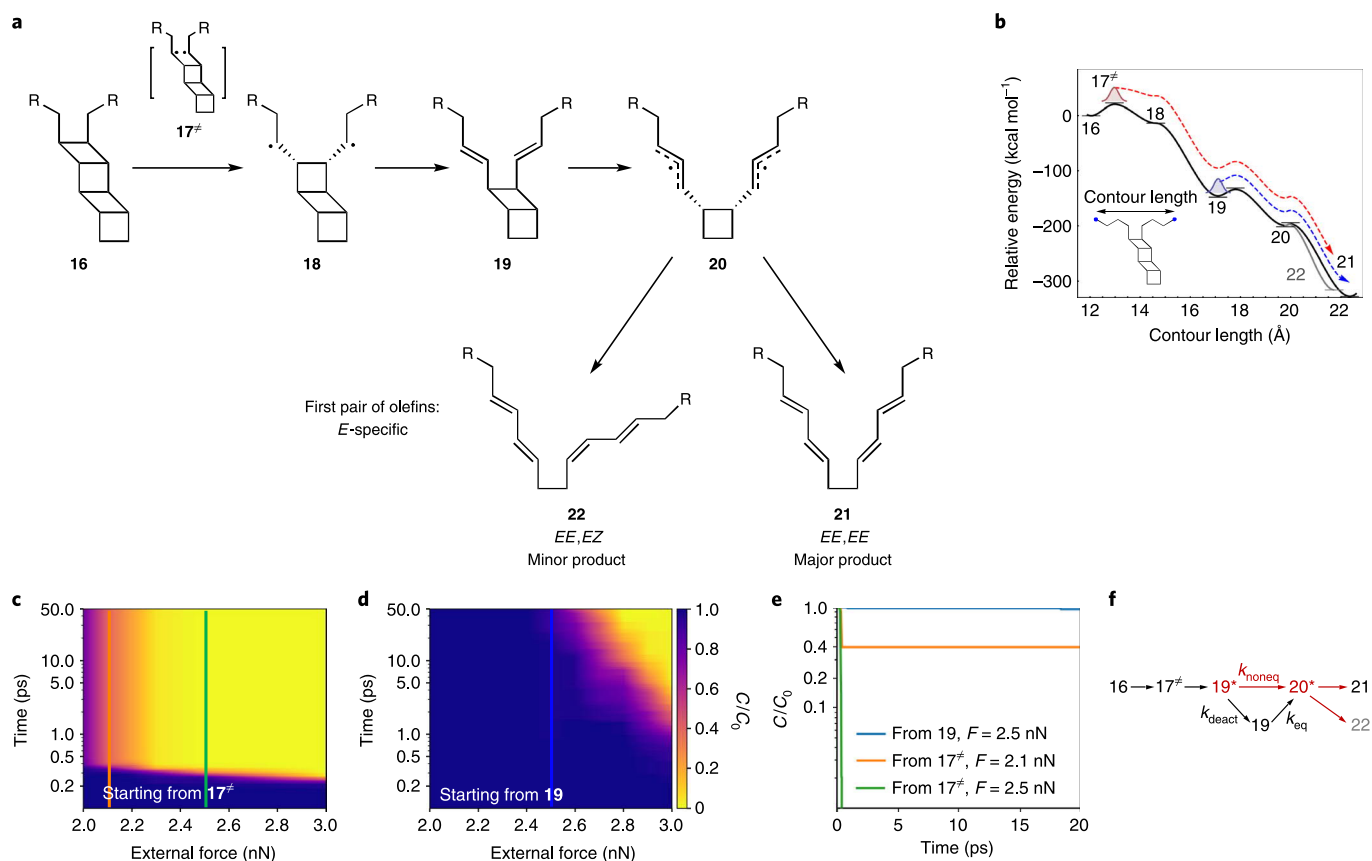


Fig. 5 | Computational analysis of the unzipping of [4]-ladderane using AISMD under different forces. **a**, Proposed mechanism of the tandem unzipping of [4]-ladderane. **b**, Energy profile along the reaction coordinate for [4]-ladderane unzipping showing all the intermediate species, obtained from minimum energy paths under 2 nN force. The red and blue dashed lines indicate the trajectories used to calculate the cycloreversion of **19** starting from optimized TS **17[#]** (red trace) or equilibrated **19** (blue trace). Contour length is the distance between the terminal atoms of the butyl groups of ladderane under 2 nN force. **c,d**, For the cycloreversion of **19**, the remaining concentration of **19** as a function of reaction time and external force, showing dramatic acceleration when starting from **17[#]** (**c**) compared with starting from equilibrated **19** (**d**), due to the dynamic effect. The fractional concentration of remaining **19** is shown using a blue (all remaining) to yellow (all opened) colour gradient. **e**, Selected cross-sections from **c** and **d** (shown by the colour-coded vertical lines) showing the changes of fractional concentration **19** over reaction time. An ultrafast reaction process followed by a statistical process is clearly visualized when the reaction starts from **17[#]**. The ultrafast process becomes more dominant at higher forces. **f**, Kinetic model of the mechanoactivation of [4]-ladderane. The red elementary steps indicate strong acceleration by dynamic effects.

Conclusions

We have investigated the mechanochemical unzipping of individual [4]-ladderane/ene structures embedded in different polymers. Although unzipping of [4]-ladderane to pentaene produced characteristic ultraviolet and Raman features for sensitive detection, [4]-ladderane allowed detailed analysis of the mechanochemical products by ¹H NMR spectroscopy. We observed cascade activation of [4]-ladderane without detectable half-unzipped intermediate. The generated dienes also exhibited interesting stereochemistry: the first cycloreversion gave only *E* olefins and the second cycloreversion gave ~80% *E* and ~20% *Z* olefins, with partial inversion from the ladderane stereochemistry.

AISMD simulations of the tandem ladderane mechanochemistry revealed non-equilibrium dynamic effects, where the kinetic energy generated from the preceding mechanochemical event is transduced to accelerate the subsequent activation by several orders of magnitude in one reaction step, and controls the stereochemical distribution of products in another step. The external forces alter the topography of the potential energy landscape, giving rise to reactive intermediates and the post-TS bifurcation of reaction pathways near a VRI point. TST predicted a stereochemical product distribution opposite to the

experimental observations, but AISMD showed excellent agreement with the experimental results, revealing a further dynamic effect. The existence of dynamic effects in multiple reaction steps during the unzipping of a single ladderane unit suggests that such effects may be ubiquitous in closely coupled tandem mechanochemical processes with decreasing barrier heights and increasing exothermicity under external force. These considerations are also important in non-mechanochemical reactions, such as photochemical processes, where dynamic effects are observed. The dynamic effect can potentially be harnessed to enable a highly desired amplification of the mechanochemical response. Additionally, we showed that experimentally relevant forces can introduce VRI points along the reaction path, suggesting the exciting possibility of controlling non-equilibrium dynamic effects by modulating forces.

Ladderane structures represent a unique framework of multi-mechanophores with well-aligned reaction coordinates and energy transduction between individual mechanoactivations, and the dynamic effects revealed herein present exciting opportunities for understanding mechanotransduction along covalent bonds and designing an amplified mechanical response using multiple coupled mechanophores.

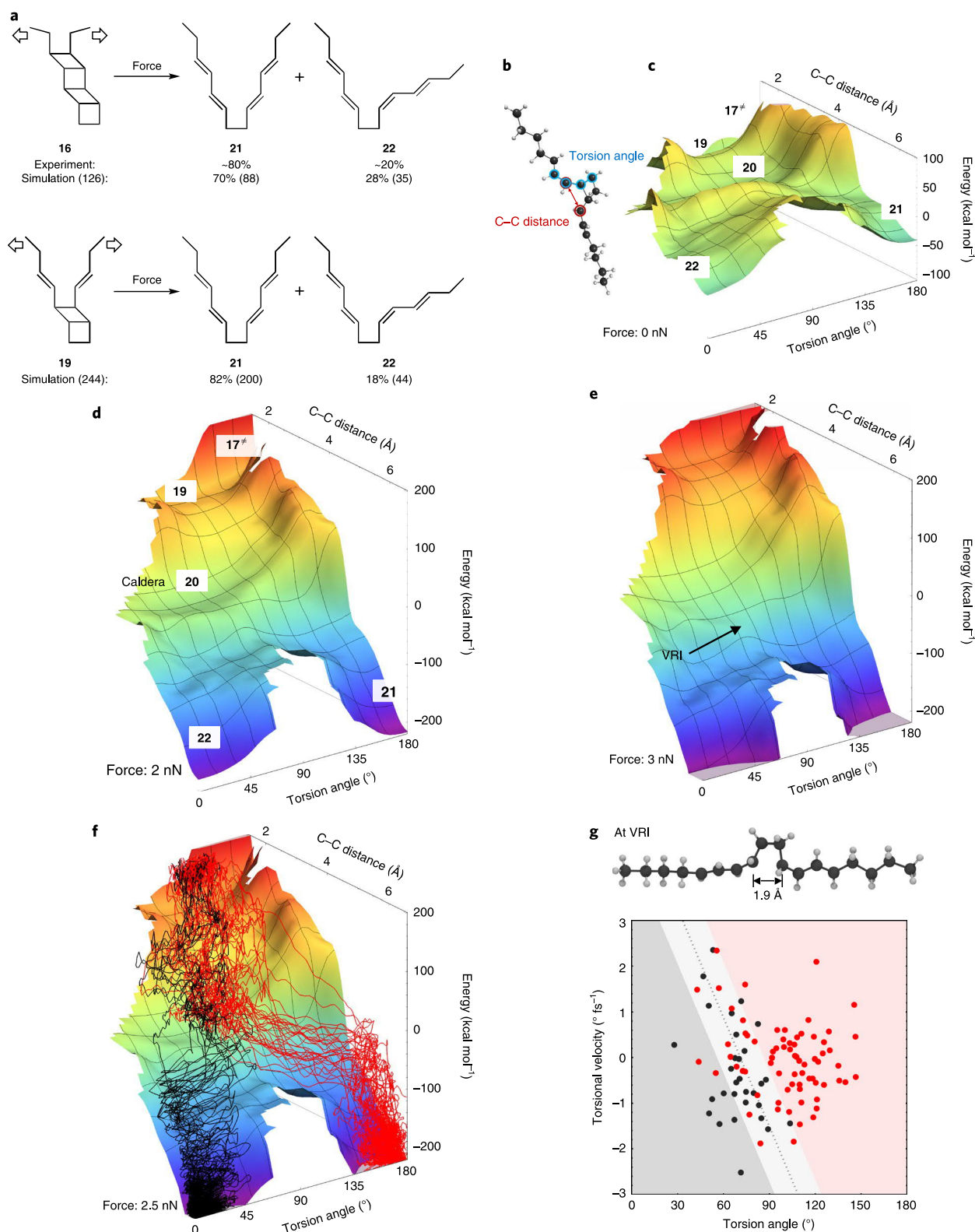


Fig. 6 | Analysis of the origin of stereochemical product distribution in the mechanochemistry of [4]-ladderane. **a**, Calculated stereochemical distribution of generated dienes, using AISMD, agrees with the experimental observations. The numbers in the parentheses represent the number of simulations. **b**, Snapshot of structure **20** on the reaction pathway, showing the breaking C-C bond distance and the dihedral torsion angle of the forming olefin (used as axes in **c-f**). **c-f**, FMPES at 0 nN (**c**), 2 nN (**d**), 2.5 nN (**f**) and 3 nN (**e**) force, showing the significantly changed topology of potential energy surfaces. In **f**, AISMD trajectories are shown that lead to products **21** (red) and **22** (black). **g**, Distribution of the torsional velocity and torsion angle when trajectories pass through the VRI region under 3 nN force, leading to products **21** (red) and **22** (black). The background colours show phase space regions correlating to each product, obtained from logistic regression, with the boundary between the two regions shown as dotted lines. The light grey area represents model prediction with <80% confidence. Trajectories start from **17[#]** and the phase space cross-section is taken at the specified bond length of 1.9 Å.

Methods

See Supplementary Information for detailed methods and protocols.

Sonochemical unzipping. Ultrasonication was performed in a 10 ml ultrasonic vessel (Ace Glass 9843–25) with a Branson 450 sonifier equipped with a 1/8 in (3 mm diameter) tapered microtip. The distance between the tip and bottom of the vessel was 1 cm. The vessel was connected to the horn with a bushing and an O-ring to ensure air-tightness. Sonication was performed using pulsed ultrasound (1.0 s on, 1.0 s off) at 20 kHz under Ar with an output of 9.2 W cm^{-2} . The vessel was placed in an ice bath or an acetonitrile dry ice bath. In the ice bath set-up, the internal temperature was measured to be $6\text{--}9^\circ\text{C}$ throughout the sonication experiments. Sonication time in this paper refers to the on time, throughout. The resulting polymer solutions were concentrated in vacuo and purified by precipitation into methanol before analysis.

Ab initio simulation. The AISMD method¹⁵ was used to simulate the mechanically induced unzipping of a single ladderane unit embedded in a polymer chain. Two *n*-butyl groups were attached to the ladderane unit, and external forces were applied at the two furthest carbon atoms, mimicking the extensional forces exerted in polymer chains under sonication (Supplementary Fig. 6). The forces on the two steered carbon atoms were collinear, of equal magnitude and in opposite directions. The AISMD simulations were performed using unrestricted density functional theory with the B3LYP functional and 6–31g* basis set using the TeraChem program suite⁴⁵. All simulations were performed in the canonical (NVT) ensemble using Langevin dynamics at 300 K (26.9°C), where the surrounding solvent was approximated as a constant-temperature external bath and facilitated energy dissipation after unzipping.

Received: 24 January 2019; Accepted: 15 November 2019;

Published online: 6 January 2020

References

- Li, J., Nagamani, C. & Moore, J. S. Polymer mechanochemistry: from destructive to productive. *Acc. Chem. Res.* **50**, 2181–2090 (2015).
- Hickenboth, C. R. et al. Biasing reaction pathways with mechanical force. *Nature* **446**, 423–427 (2007).
- Lenhardt, J. M. et al. Trapping a diradical transition state by mechanochemical polymer extension. *Science* **329**, 1057–1060 (2010).
- Piermattei, A., Karthikeyan, S. & Sijbesma, R. P. Activating catalysts with mechanical force. *Nat. Chem.* **1**, 133–137 (2009).
- Davis, D. A. et al. Force-induced activation of covalent bonds in mechanoresponsive polymeric materials. *Nature* **459**, 68–72 (2009).
- Robb, M. J. et al. Regioisomer-specific mechanochromism of naphthopyran in polymeric materials. *J. Am. Chem. Soc.* **138**, 12328–12331 (2016).
- Chen, Y. et al. Mechanically induced chemiluminescence from polymers incorporating a 1,2-dioxetane unit in the main chain. *Nat. Chem.* **4**, 559–562 (2012).
- Ducrot, E., Chen, Y., Bulters, M., Sijbesma, R. P. & Creton, C. Toughening elastomers with sacrificial bonds and watching them break. *Science* **344**, 186–189 (2014).
- Larsen, M. B. & Boydston, A. J. ‘Flex-activated’ mechanophores: using polymer mechanochemistry to direct bond bending activation. *J. Am. Chem. Soc.* **135**, 8189–8192 (2013).
- Gosswiler, G. R. et al. Mechanochemical activation of covalent bonds in polymers with full and repeatable macroscopic shape recovery. *ACS Macro Lett.* **3**, 216–219 (2014).
- Nagamani, C., Liu, H. & Moore, J. S. Mechanochemical generation of acid from oxime sulfonates. *J. Am. Chem. Soc.* **138**, 2540–2543 (2016).
- Verstraeten, F., Gostl, R. & Sijbesma, R. P. Stress-induced colouration and crosslinking of polymeric materials by mechanochemical formation of triphenylimidazolyl radicals. *Chem. Commun.* **52**, 8608–8611 (2016).
- Imato, K. et al. Repeatable mechanochemical activation of dynamic covalent bonds in thermoplastic elastomers. *Chem. Commun.* **52**, 10482–10485 (2016).
- Klukovich, H. M., Kouznetsova, T. B., Kean, Z. S., Lenhardt, J. M. & Craig, S. L. A backbone lever-arm effect enhances polymer mechanochemistry. *Nat. Chem.* **5**, 110–114 (2013).
- Ong, M. T., Leiding, J., Tao, H., Virshup, A. M. & Martínez, T. J. First principles dynamics and minimum energy pathways for mechanochemical ring opening of cyclobutene. *J. Am. Chem. Soc.* **131**, 6377–6379 (2009).
- Chen, Z. et al. Mechanochemical unzipping of insulating poly(ladderene) to semiconducting polyacetylene. *Science* **357**, 475–479 (2017).
- Hermes, M. & Boulatov, R. The entropic and enthalpic contributions to force-dependent dissociation kinetics of the pyrophosphate bond. *J. Am. Chem. Soc.* **133**, 20044–20047 (2011).
- Akbulatov, S. et al. Experimentally realized mechanochemistry distinct from force-accelerated scission of loaded bonds. *Science* **357**, 299–303 (2017).
- Kryger, M. J. et al. Masked cyanoacrylates unveiled by mechanical force. *J. Am. Chem. Soc.* **132**, 4558–4559 (2010).
- Kryger, M. J., Munaretto, A. M. & Moore, J. S. Structure–mechanochemical activity relationships for cyclobutane mechanophores. *J. Am. Chem. Soc.* **133**, 18992–18998 (2011).
- Klukovich, H. M., Kean, Z. S., Iacono, S. T. & Craig, S. L. Mechanically induced scission and subsequent thermal remodeling of perfluorocyclobutane polymers. *J. Am. Chem. Soc.* **133**, 17882–17888 (2011).
- Kean, Z. S., Black Ramirez, A. L., Yan, Y. & Craig, S. L. Bicyclo[3.2.0]heptane mechanophores for the non-scissile and photochemically reversible generation of reactive bis-enones. *J. Am. Chem. Soc.* **134**, 12939–12942 (2012).
- Kean, Z. S., Niu, Z., Hewage, G. B., Rheingold, A. L. & Craig, S. L. Stress-responsive polymers containing cyclobutane core mechanophores: reactivity and mechanistic insights. *J. Am. Chem. Soc.* **135**, 13598–13604 (2013).
- Robb, M. J. & Moore, J. S. A retro-Staudinger cycloaddition: mechanochemical cycloelimination of a beta-lactam mechanophore. *J. Am. Chem. Soc.* **137**, 10946–10949 (2015).
- Wang, J., Kouznetsova, T. B., Boulatov, R. & Craig, S. L. Mechanical gating of a mechanochemical reaction cascade. *Nat. Commun.* **7**, 13433 (2016).
- Bowser, B. H. & Craig, S. L. Empowering mechanochemistry with multi-mechanophore polymer architectures. *Polym. Chem.* **9**, 3583–3593 (2018).
- Naylor, P. & Whiting, M. C. Researches on polyenes. Part III. The synthesis and light absorption of dimethylpolyenes. *J. Chem. Soc.* 3037–3047 (1955).
- Thompson, L. H. & Doraiswamy, L. K. Sonochemistry: science and engineering. *Ind. Eng. Chem. Res.* **38**, 1215–1249 (1999).
- El-Agamey, A. et al. Carotenoid radical chemistry and antioxidant/pro-oxidant properties. *Arch. Biochem. Biophys.* **430**, 37–48 (2004).
- Schügerl, F. B. & Kuzmany, H. Optical modes of *trans*-polyacetylene. *J. Chem. Phys.* **74**, 953–958 (1981).
- Knoll, K. & Schrock, R. R. Preparation of *tert*-butyl-capped polyenes containing up to 15 double bonds. *J. Am. Chem. Soc.* **111**, 7989–8004 (1989).
- Ribas-Arino, J., Shiga, M. & Marx, D. Mechanochemical transduction of externally applied forces to mechanophores. *J. Am. Chem. Soc.* **132**, 10609–10614 (2010).
- Carpenter, B. K. Nonstatistical dynamics in thermal reactions of polyatomic molecules. *Annu. Rev. Phys. Chem.* **56**, 57–89 (2005).
- Carpenter, B. K. Energy disposition in reactive intermediates. *Chem. Rev.* **113**, 7265–7286 (2013).
- Oyola, Y. & Singleton, D. A. Dynamics and the failure of transition state theory in alkene hydroboration. *J. Am. Chem. Soc.* **131**, 3130–3131 (2009).
- Bailey, J. O. & Singleton, D. A. Failure and redemption of statistical and nonstatistical rate theories in the hydroboration of alkenes. *J. Am. Chem. Soc.* **139**, 15710–15723 (2017).
- Doering, W. E., Cheng, X., Lee, K. & Lin, Z. Fate of the intermediate diradicals in the caldera: stereochemistry of thermal stereomutations, (2+2) cycloreversions, and (2+4) ring-enlargements of *cis*- and *trans*-1-cyano-2-(*E* and *Z*)-propenyl-*cis*-3,4-dideuteriocyclobutanes. *J. Am. Chem. Soc.* **124**, 11642–11652 (2002).
- Collins, P., Kramer, Z. C., Carpenter, B. K., Ezra, G. S. & Wiggins, S. Nonstatistical dynamics on the caldera. *J. Chem. Phys.* **141**, 034111 (2014).
- Grimme, S. Supramolecular binding thermodynamics by dispersion-corrected density functional theory. *Chem. Eur. J.* **18**, 9955–9964 (2012).
- Doubleday, C., Suhrada, C. P. & Houk, K. N. Dynamics of the degenerate rearrangement of bicyclo[3.1.0]hex-2-ene. *J. Am. Chem. Soc.* **128**, 90–94 (2006).
- Ess, D. H. Bifurcations on potential energy surfaces of organic reactions. *Angew. Chem. Int. Ed.* **47**, 7592–7601 (2008).
- Hare, S. R. & Tantillo, D. J. Post-transition state bifurcations gain momentum—current state of the field. *Pure Appl. Chem.* **89**, 679–698 (2017).
- Wollenhaupt, M., Schran, C., Krupička, M. & Marx, D. Force-induced catastrophes on energy landscapes: mechanochemical manipulation of downhill and uphill bifurcations explains the ring-opening selectivity of cyclopropanes. *ChemPhysChem* **19**, 837–847 (2018).
- Lee, B., Niu, Z., Wang, J., Slebodnick, C. & Craig, S. L. Relative mechanical strengths of weak bonds in sonochemical polymer mechanochemistry. *J. Am. Chem. Soc.* **137**, 10826–10832 (2015).
- Ufimtsev, I. S. & Martínez, T. J. Quantum chemistry on graphical processing units. 3. Analytical energy gradients, geometry optimization and first principles molecular dynamics. *J. Chem. Theory Comput.* **5**, 2619–2628 (2009).

Data availability

Optimized geometries for the structures discussed in the text are available in the supplementary files in the online version of the paper. The experimental and simulation data that support the findings of this study are available from the authors upon request.

Code availability

The program TeraChem (v1.92), used for steered ab initio molecular dynamics calculations and reaction path optimization, is available from PetaChem, LLC (<http://www.petachem.com/products.html>). The scripts used to analyse the trajectories are available upon request from T.J.M.

Acknowledgements

This work was supported by the US Army Research Office under grant no. W911NF-15-1-0525. J.A.M.M. thanks the National Science Foundation for a graduate fellowship. T.J.M. acknowledges support from Office of Naval Research grant no. N00014-12-1-0828. This work used the XStream computational resource supported by the National Science Foundation Major Research Instrumentation programme (ACI-1429830). We thank B. M. Trost for the use of the ozone generator and S. R. Lynch for advice on NMR spectroscopy.

Author contributions

Z.C., X.Z., T.J.M. and Y.X. conceived this project. Z.C. and Y.X. designed the experiments and X.Z. and T.J.M. designed the computations. Z.C. and J.Y. prepared the polymers and performed the mechanoactivation, characterizations and data analysis, under the guidance of Y.X. X.Z. performed calculations and data analysis under the guidance of T.J.M. J.A.M.M. synthesized starting materials **1** and **8** under the guidance of N.Z.B. Z.C., X.Z. and Y.X. wrote the manuscript. All authors discussed the results and commented on the manuscript.

Competing interests

The authors declare no competing interests.

Additional information

Correspondence and requests for materials should be addressed to T.J.M. or Y.X.